

## *Supporting Information*

# *In situ* Fabrication of Nanoprobes for $^{19}\text{F}$ Magnetic Resonance Imaging and Photoacoustic Imaging Guided Tumor Therapy

Chang Guo<sup>#</sup>, Yunhe Yan<sup>#</sup>, Suying Xu\* and Leyu Wang\*

State Key Laboratory of Chemical Resource Engineering, Beijing Advanced Innovation Center for Soft Matter Science and Engineering, College of Chemistry, Beijing University of Chemical Technology; Beijing, 100029, China

## List of content

**Figure S1:** The zeta potentials of CuS, CFP, CFPP, respectively.

**Figure S2:** Energy-dispersive X-ray spectroscopy (EDS) of CFPP NPs.

**Figure S3:** TEM images of CFPP NPs prepared under different temperatures (50-80 °C), respectively.

**Figure S4:** TEM images of CFPP NPs prepared by adding different concentrations of sodium sulphide (3.0-8.0 mM), respectively.

**Figure S5:** HRTEM image of the d-CFPP NPs. The inserted image is an enlarged area.

**Figure S6:** Photothermal images of CFPP NPs, d-CFPP NPs and water along with illumination by 1064-nm laser.

**Figure S7:** Photothermal performance curve of CFPP NPs with different concentrations.

**Figure S8:** Photothermal effect of CFPP NPs upon five cycles by switching the laser on/off.

**Figure S9:** Size distributions and  $^{19}\text{F}$  SNR intensity evolution of CFPP NPs after incubation in FBS or Balb/C mouse blood serum at 37 °C for 7 days.

**Table S1:** Stability tests of CFPP NPs

**Figure S10:**  $^{19}\text{F}$  NMR intensities of 4T1 cells lysates after incubation with CFPP for different time intervals.

**Figure S11:** Temperature evolution profile of mice after injection of CFPP NPs at 2 h, 4 h, 6 h, 8 h and 24 h, respectively.

**Figure S12:** The plot of the  $^{19}\text{F}$  MRI signal-to-noise ratio (SNR) *versus* CFPP NPs concentration.

**Figure S13:** *In vivo*  $^1\text{H}$  and  $^{19}\text{F}$  MRI images of the tumor-bearing mice at different time intervals after intravenous injection of CFPPs (i.v.). (a-d) represent 1 h, 4 h, 24 h, 48 h, respectively.

**Figure S14:** *In vivo* PA signals of tumor site at different times after intravenous of CFPP NPs.

**Figure S15:** Release curves of PTX for CFPP NPs under different pH conditions.

**Figure S16:** The release percentages of PTX for CFPP NPs under different conditions after dialysis for 6 hours.

**Figure S17:** H&E-stained slices of different tissues from different groups. Scale bar: 50  $\mu\text{m}$ . (i) PBS, (v) CFPP NPs + Laser.

**Figure S18:** The mice blood biochemistry assay data. ( $n = 3$ )

**Figure S19:** The mice liver and kidney function blood tests. ( $n = 3$ )

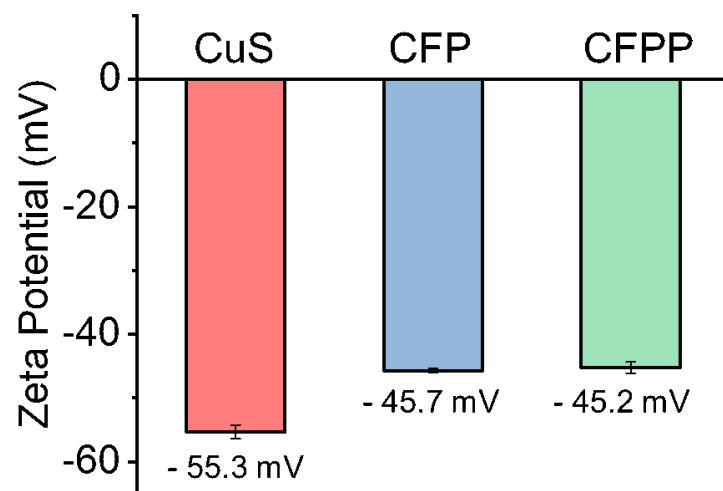


**Figure S1.** The zeta potential of CuS, CFP, CFPP, respectively.

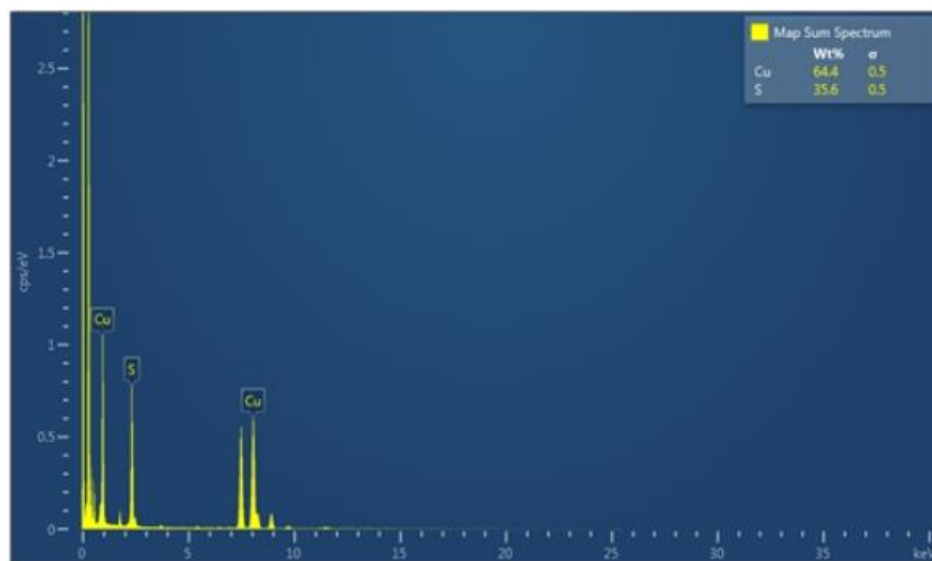


**Figure S2.** Energy-dispersive X-ray spectroscopy (EDS) of CFPP NPs.

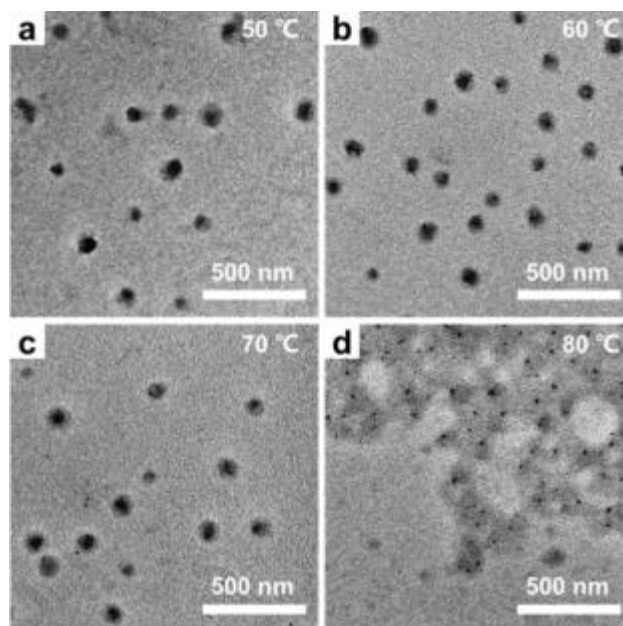


**Figure S3.** TEM images of CFPP NPs prepared under different temperatures (50-80°C), respectively. (a-d) represent 50°C, 60 °C , 70 °C and 80 °C, respectively.

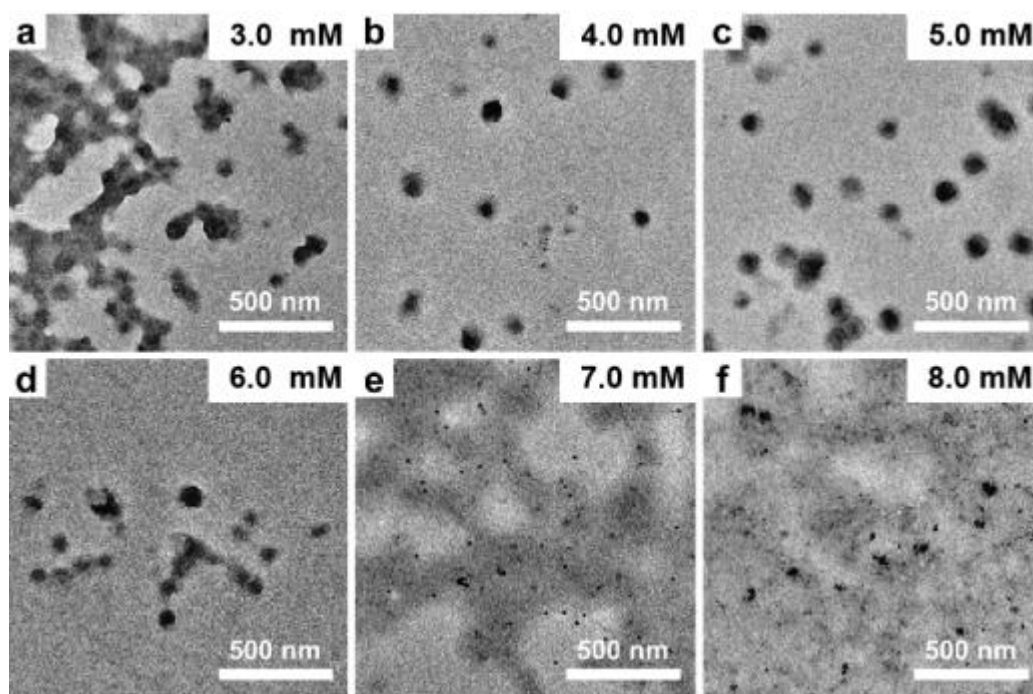


**Figure S4.** TEM images of CFPP NPs prepared by adding different concentrations of sodium sulphide (3.0-8.0 mM), respectively. (a-f) represent 3.0 mM, 4.0 mM, 5.0 mM, 6.0 mM, 7.0 mM and 8.0 mM, respectively.

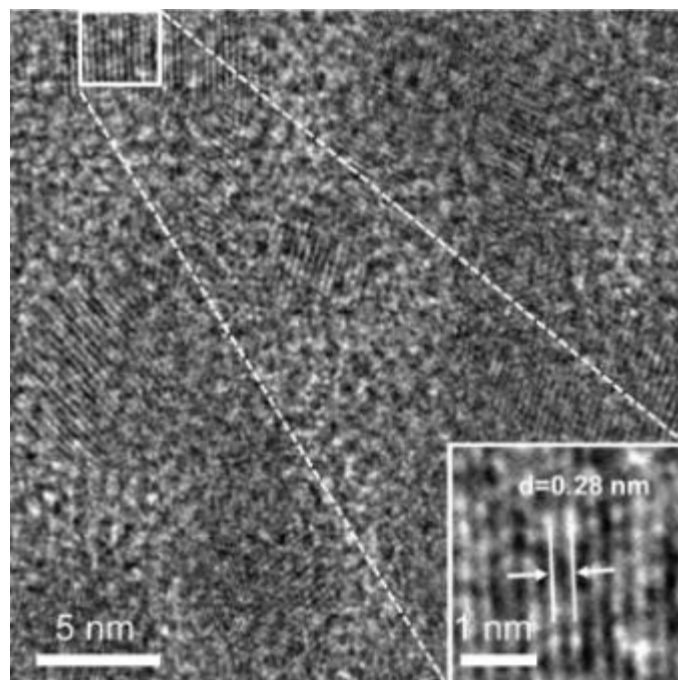


**Figure S5.** HRTEM image of the d-CFPP NPs. The inserted image is an enlarged area.

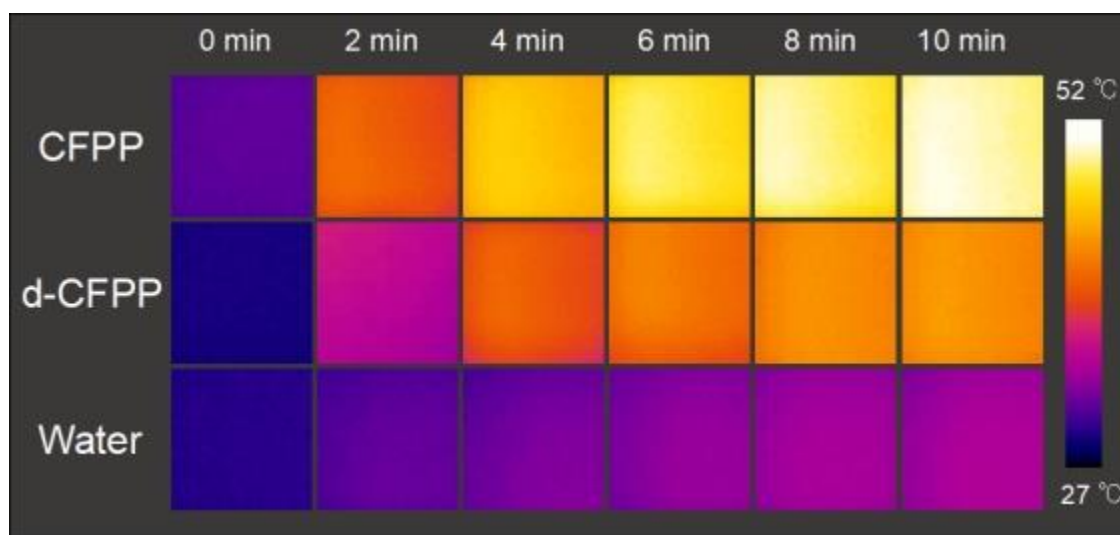


**Figure S6.** Photothermal images of CFPP NPs, d-CFPP NPs and water along with illumination by 1064-nm laser.

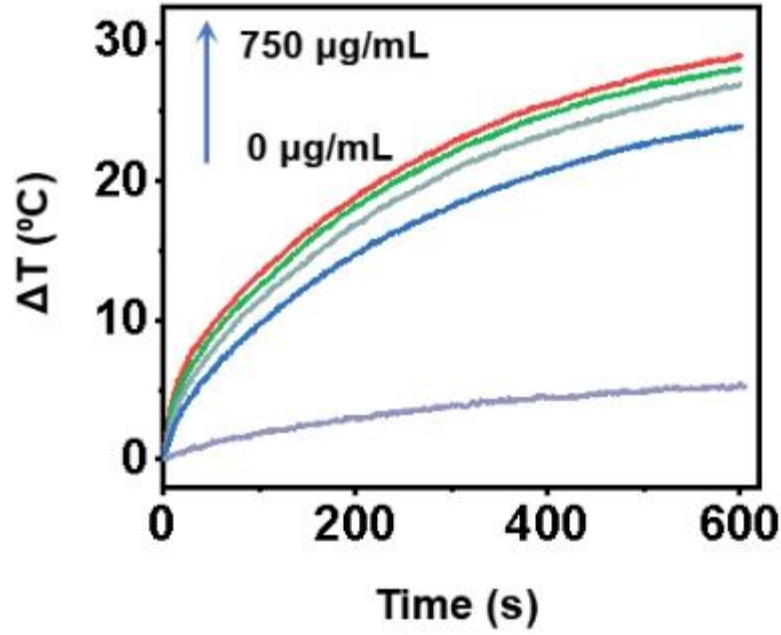


**Figure S7.** Photothermal performance curve of CFPP NPs with different concentrations (750  $\mu\text{g/mL}$ , 500  $\mu\text{g/mL}$ , 250  $\mu\text{g/mL}$ , 125  $\mu\text{g/mL}$ , 0  $\mu\text{g/mL}$ ).

#### Calculation of the Photothermal Conversion Efficiency:

The calculation of the photothermal conversion efficiency ( $\eta$ ) is based on the previous work,<sup>[1-2]</sup> using the following series of formulas:

$$Q_{NPs} = I(1 - 10^{-A_\lambda})\eta \quad (\text{S1})$$

$$\sum_i m_i C_{p,i} \frac{dT}{dt} = Q_{NPs} + Q_s - Q_{loss} \quad (\text{S2})$$

$C_p$  and  $m$  are the heat capacity and mass,  $T$  is the solution temperature.  $Q_{NPs}$  is the photothermal energy absorbed by nanoparticles per second,  $Q_s$  is the heat associated with the light absorbed by solvent per second and  $Q_{loss}$  is thermal energy lost to the surroundings.

$$Q_{loss} = hA \Delta T \quad (\text{S3})$$

$I$  is the laser power,  $A_\lambda$  is the absorbance of NPs in an aqueous solution. In this system, the absorption of NPs at 1064nm was selected.  $h$  is the heat transfer coefficient,  $A$  is the surface area of the container, and  $\Delta T$  is the changed temperature, which is referred to  $T - T_{amb}$ .

In a dispersed system of water, the heat input is equal to the heat output at the maximum steady-state temperature:

$$Q_S = Q_{loss} = hA \Delta T_{max, H_2O} \quad (S4)$$

In a dispersed system of nanoparticles, the heat inputs are the heat generated by nanoparticles ( $Q_{NPs}$ ) and the heat generated by water ( $Q_S$ ), which is equal to the heat output at the maximum steady-state temperature:

$$Q_{NPs} + Q_S = Q_{loss} = hA \Delta T_{max, mix} \quad (S5)$$

Thus, the formula for calculating the photothermal conversion efficiency can be derived:

$$\eta = \frac{hA(\Delta T_{max, mix} - \Delta T_{max, H_2O})}{I(1 - 10^{-A_\lambda})} \quad (S6)$$

To get the  $hA$ , we introduce  $\theta$ , which is defined as the ratio of  $\Delta T$  to  $\Delta T_{max}$

$$\theta = \frac{T_{amb} - T}{T_{amb} - T_{max}} \quad (S7)$$

Substituting equation (S7) into equation (S2):

$$\frac{d\theta}{dt} = \frac{hA}{\sum_i m_i C_{p,i}} \left( \frac{Q_{NPs} + Q_S}{hA \Delta T_{max}} - \theta \right) \quad (S8)$$

When the laser is removed,

$$Q_{NPs} + Q_S = 0 \quad (S9)$$

$$dt = -\frac{\sum_i m_i C_{p,i}}{hA} \frac{d\theta}{\theta} \quad (\text{S10})$$

$$t = -\frac{\sum_i m_i C_{p,i}}{hA} \ln \theta \quad (\text{S11})$$

$\tau_s$  can be introduced to represent  $\frac{\sum_i m_i C_{p,i}}{hA}$ , which means the sample system time constant.

Therefore,  $hA$  can be obtained through linear fitting the graph of  $\tau_s$  against  $-\ln \theta$ . Then  $\eta$  can be obtained.

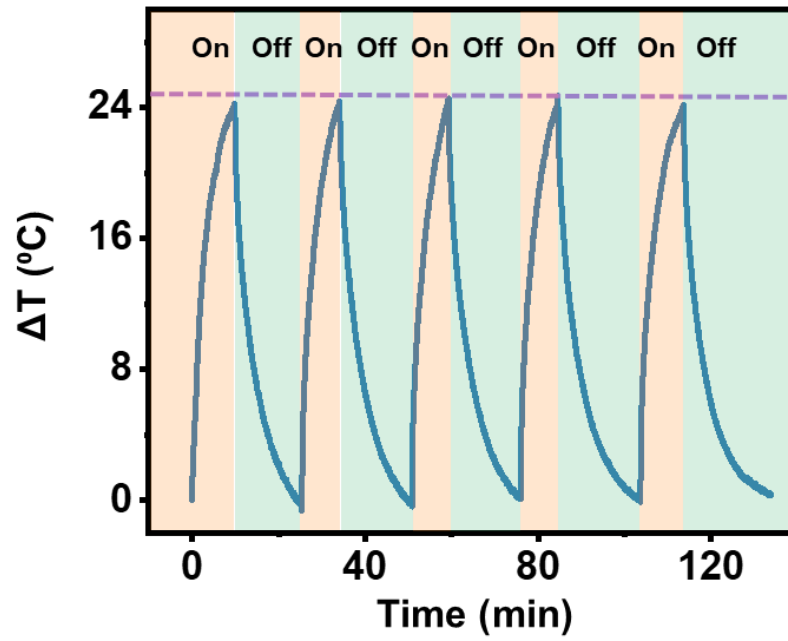


**Figure S8.** The photothermal effect of CFPP NPs (500 µg/mL) upon five cycles by switching the laser on/off.



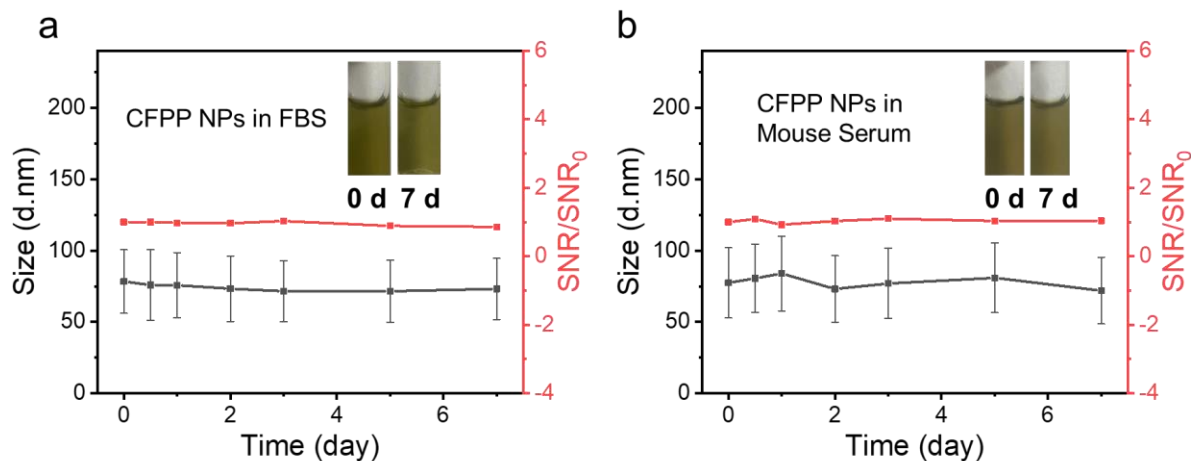


**Figure S9.** Size distributions and  $^{19}\text{F}$  SNR intensity evolution of CFPP NPs after incubation in FBS (a) or Balb/C mouse blood serum (b) at  $37^\circ\text{C}$  for 7 days

**Table S1.** Stability tests of CFPP NPs

Time Time (day)	Chemical shift (ppm) of $^{19}\text{F}$ NMR	Signal-to-noise ratio (SNR) of $^{19}\text{F}$ NMR	Peak width at half height (Hz) of $^{19}\text{F}$ NMR	Dynamic light scattering (DLS) size in water (nm)	Dynamic light scattering (DLS) size in PBS (nm)
0	-91.87	8621.33	18.59	$77.64 \pm 20.99$	$72.47 \pm 20.57$
7	-91.89	9260.18	18.40	$78.60 \pm 20.66$	$74.18 \pm 19.48$
14	-91.91	8934.21	17.43	$78.76 \pm 20.59$	$70.35 \pm 19.41$
21	-91.90	9188.66	17.51	$73.88 \pm 20.08$	$71.49 \pm 21.32$
28	-91.90	8647.61	17.00	$70.63 \pm 19.67$	$70.58 \pm 19.39$

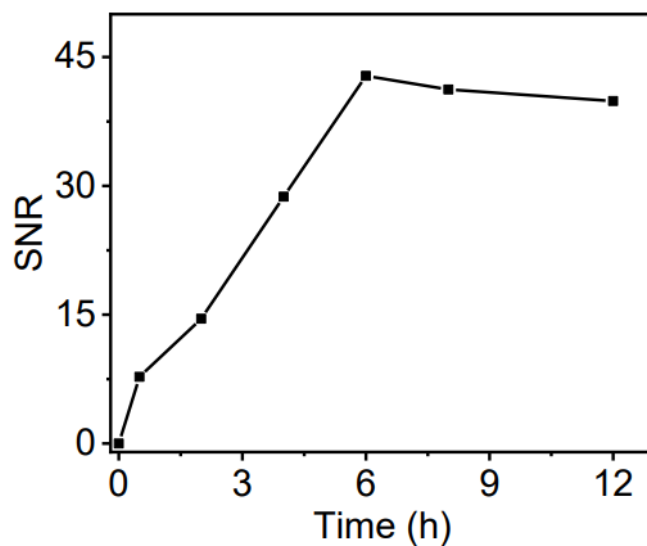


**Figure S10:**  $^{19}\text{F}$  NMR spectra of 4T1 cells lysates after incubation with CFPP for different time intervals.

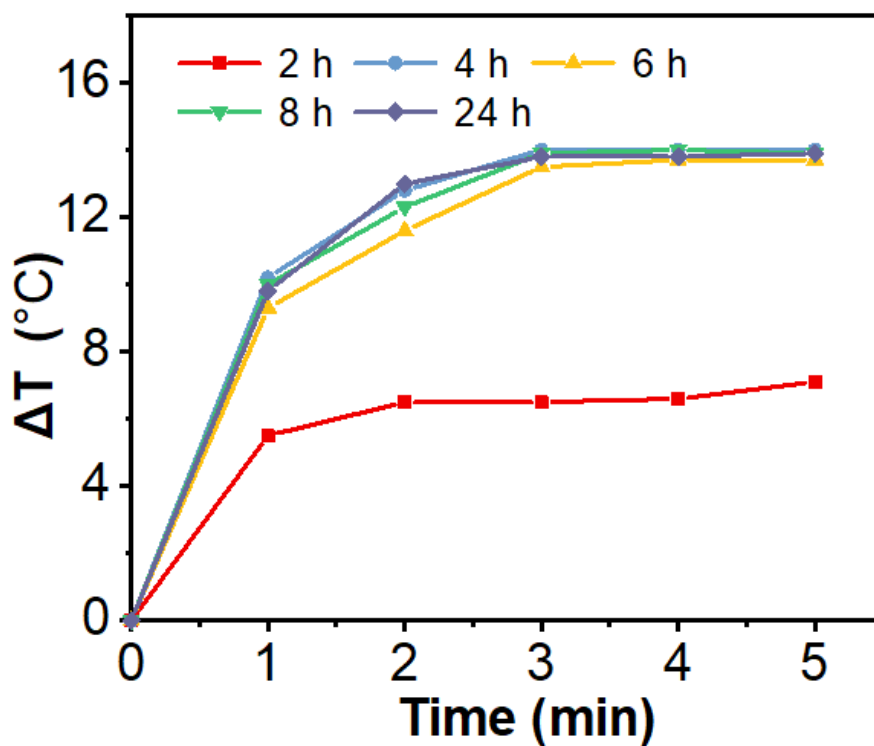


**Figure S11:** Temperature evolution profile of mice after injection of CFPP NPs at 2 h, 4 h, 6 h, 8 h and 24 h, respectively.

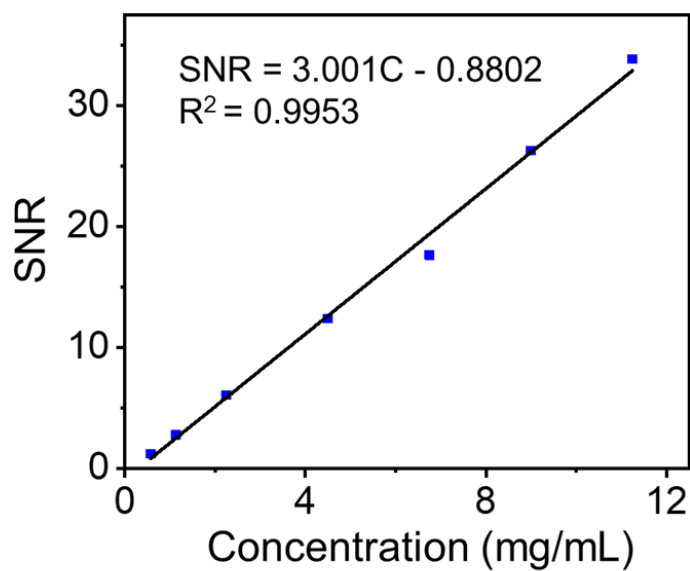


**Figure S12.** The plot of the  $^{19}\text{F}$  MRI signal-to-noise ratio (SNR) *versus* CFPP NPs concentration.

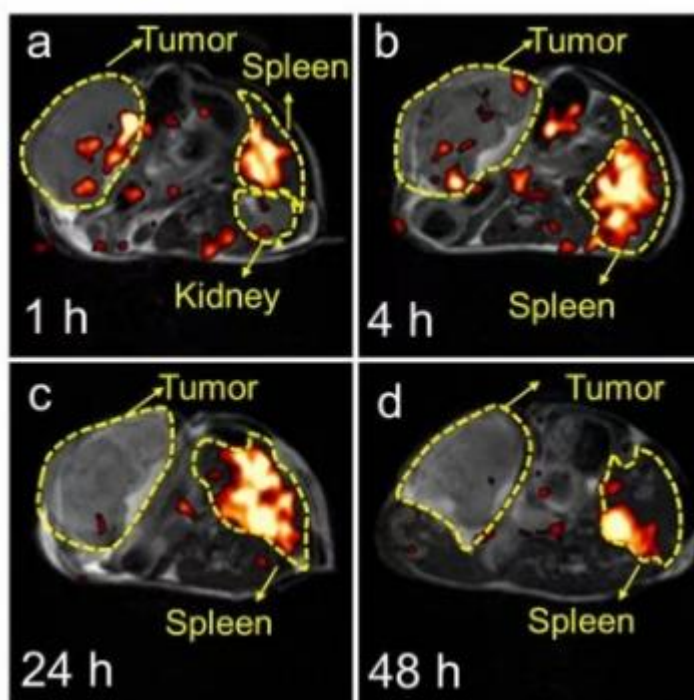


**Figure S13.** *In vivo*  $^1\text{H}$  and  $^{19}\text{F}$  MRI images of the tumor-bearing mice at different time intervals after intravenous injection of CFPPs (i.v.). (a-d) represent 1, 4, 24 and 48 h, respectively.

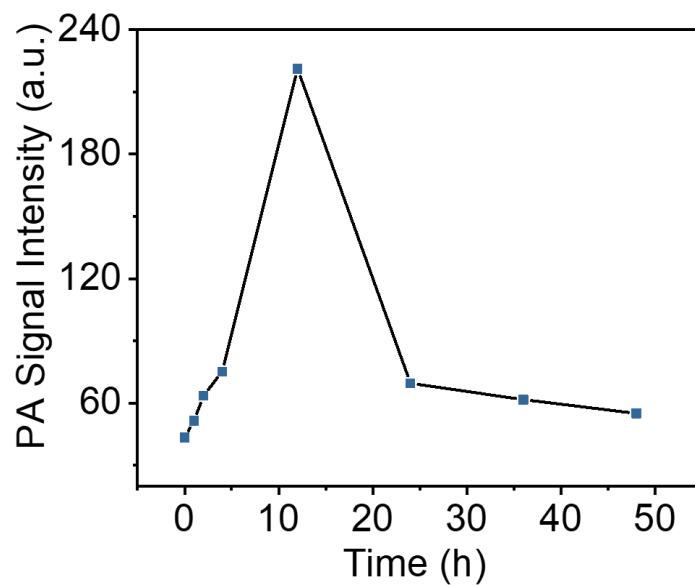


**Figure S14.** *In vivo* PA signals of tumor site at different time after intravenous of CFPP NPs.

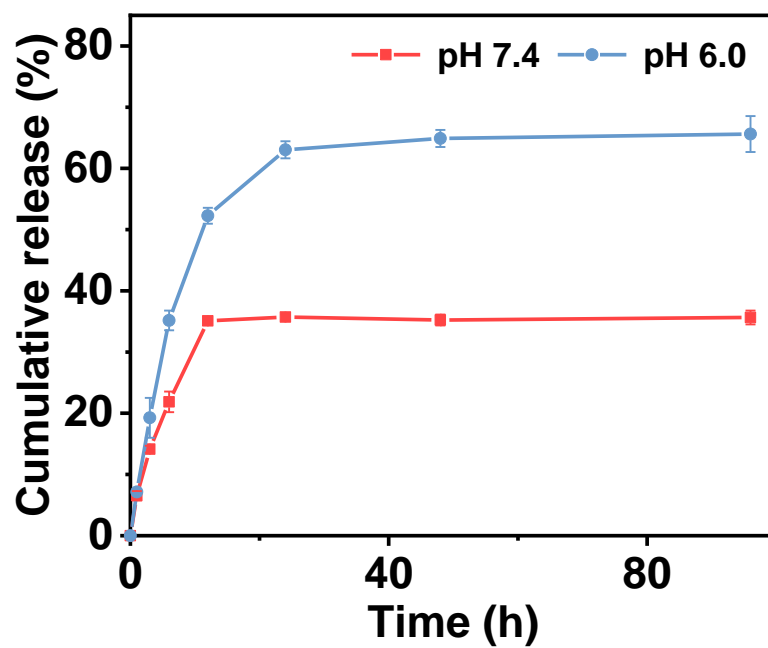


**Figure S15.** Release curves of PTX for CFPP NPs under different pH conditions.

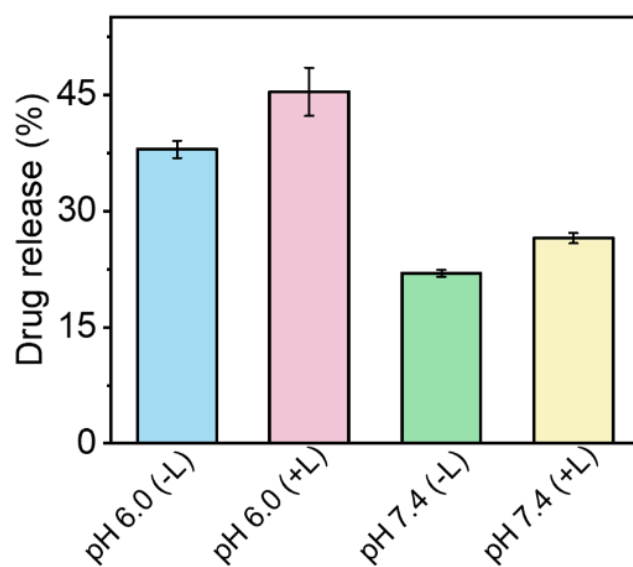


**Figure S16.** The release percentages of PTX for CFPP NPs under different conditions after dialysis for 6 hours.

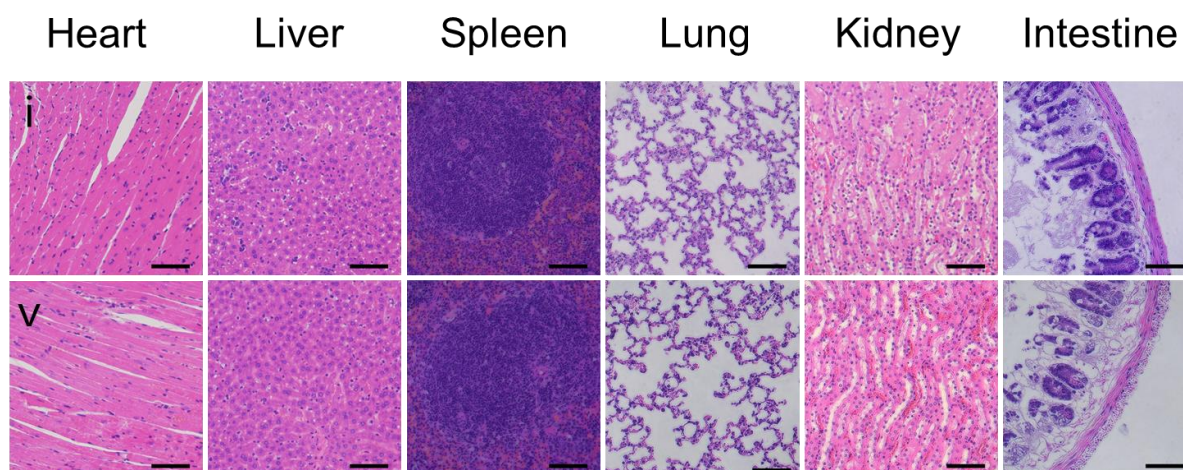


**Figure S17.** H&E-stained slices of different tissues from different groups. Scale bar: 50  $\mu\text{m}$ . (i) PBS, (v) CFPP NPs + Laser.

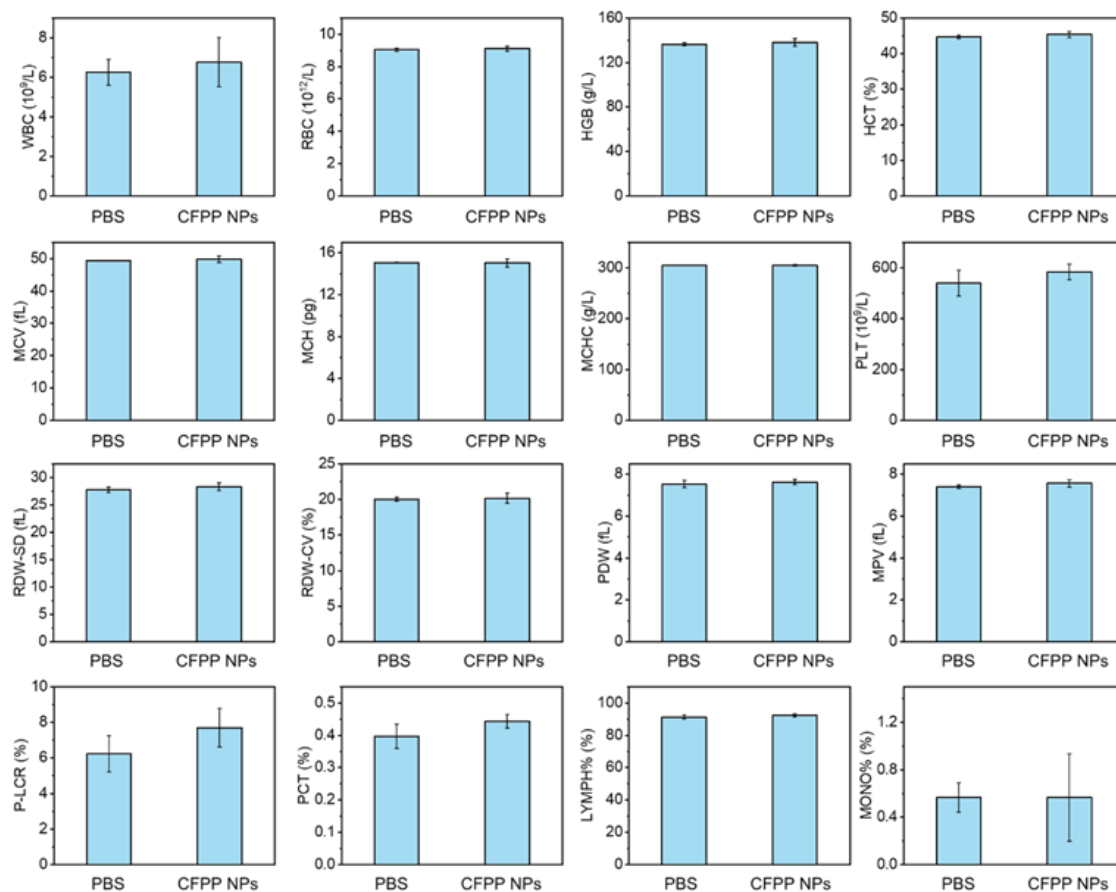


**Figure S18.** The mice blood biochemistry assay data. (n = 3)

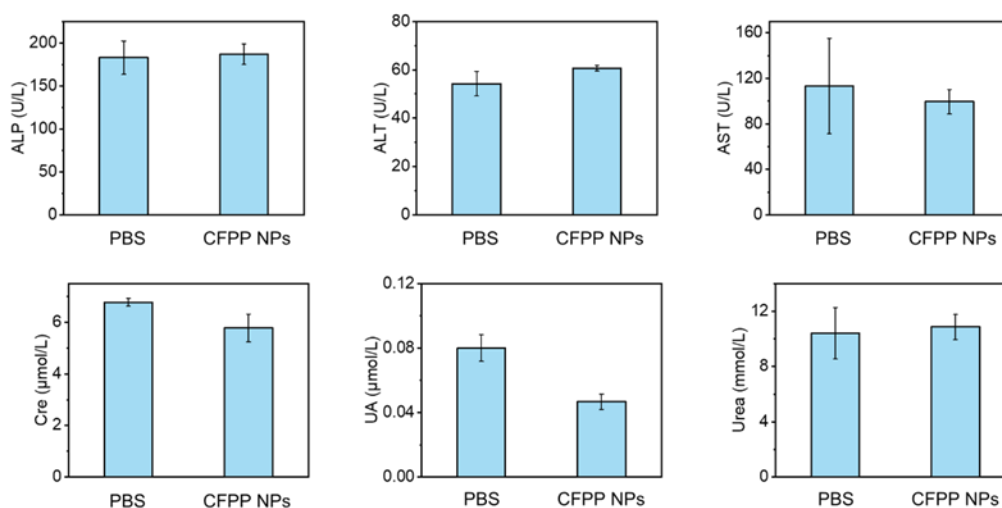


**Figure S19.** The mice liver and kidney function blood tests. (n = 3)

## References

- [1] Ren, W. Z.; Yan, Y.; Zeng, L. Y.; Shi, Z. Z.; Gong, A.; Schaaf, P.; Wang, D.; Zhao, J. S.; Zou, B. B.; Yu, H. S.; Chen, G.; Brown, E. M. B.; Wu, A. G. *Adv. Healthc. Mater.* **2015**, *4*, 1526-1536.
- [2] Roper, D. K.; Ahn, W.; Hoepfner, M. *J. Phys. Chem. C* **2007**, *111*, 3636-3641.